

## EVOLUTION OF THE MASS AND LUMINOSITY FUNCTIONS OF GLOBULAR STAR CLUSTERS

PAUL GOUDFROOIJ AND S. MICHAEL FALL

Space Telescope Science Institute, 3700 San Martin Drive, Baltimore, MD 21218, USA; [goudfroo@stsci.edu](mailto:goudfroo@stsci.edu)  
To appear in *ApJ*, 833, 8 (2016)

### ABSTRACT

We reexamine the dynamical evolution of the mass and luminosity functions of globular star clusters (GCMF and GCLF). Fall & Zhang (2001, hereafter FZ01) showed that a power-law MF, as commonly seen among young cluster systems, would evolve by dynamical processes over a Hubble time into a peaked MF with a shape very similar to the observed GCMF in the Milky Way and other galaxies. To simplify the calculations, the semi-analytical FZ01 model adopted the “classical” theory of stellar escape from clusters, and neglected variations in the  $M/L$  ratios of clusters. Kruijssen & Portegies Zwart (2009, hereafter KPZ09) modified the FZ01 model to include “retarded” and mass-dependent stellar escape, the latter causing significant  $M/L$  variations. KPZ09 asserted that their model was compatible with observations whereas the FZ01 model was not. We show here that this claim is not correct; the FZ01 and KPZ09 models fit the observed Galactic GCLF equally well. We also show that there is no detectable correlation between  $M/L$  and  $L$  for GCs in the Milky Way and Andromeda galaxies, in contradiction with the KPZ09 model. Our comparisons of the FZ01 and KPZ09 models with observations can be explained most simply if stars escape at rates approaching the classical limit for high-mass clusters, as expected on theoretical grounds.

*Keywords:* galaxies: star clusters: general — Galaxy: kinematics and dynamics — globular clusters: general

### 1. INTRODUCTION

One of the most remarkable properties of globular cluster (GC) systems is the similarity of their luminosity functions from one galaxy to another. These have bell-like shapes and are often modeled as log-normal distributions of luminosities or, equivalently, Gaussian distributions of magnitudes (see, e.g., Harris 1991). In contrast, the luminosity functions of young cluster systems are always found to be power laws,  $\phi(L) = dN/dL \propto L^\alpha$  with  $\alpha \approx -2$  (van den Bergh & Lafontaine 1984; Elson & Fall 1985; Christian & Schommer 1988; see Whitmore et al. 2014 for a recent comprehensive study of 20 star-forming galaxies).

The mass functions of cluster systems have greater dynamical significance than their luminosity functions. For systems of old, coeval clusters, variations in the mass-to-light ( $M/L$ ) ratios are relatively small, and the luminosity function is a good proxy for the mass function. Thus, the mass function of globular clusters (GCMF) must have nearly the same bell-like shape as the luminosity function (GCLF). However, systems of young clusters in the process of formation have wide spreads in  $M/L$ , and the mass function must be determined separately from the luminosity function, usually by estimating the masses, ages, and reddenings of individual clusters in the sample from multi-band photometry. (See Fall 2006 for the mathematical relations between the mass, luminosity, and age distributions of cluster systems.) Studies of this kind show that the mass functions of young cluster systems are power laws,  $\psi(M) = dN/dM \propto M^\beta$  with  $\beta \approx -2$  (Zhang & Fall 1999; Fall & Chandar 2012, and references therein). As a consequence, larger systems of young clusters will contain more massive clusters, reaching  $M \sim 10^6 M_\odot$  or even  $\sim 10^7 M_\odot$  in some cases (Chandar et al. 2010). The most massive of these clusters are often referred to as “young GCs”.

There are two possible explanations for the radically different mass functions of young and old cluster systems: either (1) the process of cluster formation, and hence the initial cluster mass function, differed in the distant past from the present,

or (2) the mass function of clusters evolves by dynamical processes from an initial power law into a bell-shaped distribution. The second possibility—the one we examine in this paper—has been explored at various levels of approximation over the years (Fall & Rees 1977; Gnedin & Ostriker 1997; Baumgardt 1998; Vesperini 1998; Prieto & Gnedin 2008). We focus here on the semi-analytical model for the evolution of the mass function developed by Fall & Zhang (2001, hereafter FZ01).

In the FZ01 model, clusters are tidally limited at the pericenters of their galactic orbits and are disrupted by the gradual escape of stars driven by a combination of internal two-body relaxation and external gravitational shocks. For most clusters, shocks are relatively weak, and relaxation is the dominant disruption mechanism. According to the “classical” theory of relaxation-driven stellar escape, as formulated by Spitzer (1987) and others, the mass  $M$  of a tidally limited cluster decreases at a nearly constant rate:  $dM/dt = \mu$  with  $\mu \propto \rho_h^{1/2}$ , where  $\rho_h = 3M/(8\pi r_h^3)$  is the mean density within the half-mass radius  $r_h$  of the cluster. FZ01 showed that, in this approximation, the evolving GCMF at any time  $\psi(M, t)$  is related to the initial GCMF  $\psi_0(M)$  by  $\psi(M, t) = \psi_0(M + \mu t)$ . This has a characteristic bend or peak at  $M \sim \mu t$  and the limiting forms  $\psi(M, t) = \psi_0(\mu t)$ , independent of  $M$  for  $M \ll \mu t$ , and  $\psi(M, t) = \psi_0(M)$ , independent of  $t$  for  $M \gg \mu t$ .

FZ01 compared their model to the observed GCLF in the Milky Way in the approximation of constant  $M/L$  and found excellent agreement. In particular, they showed both theoretically and observationally, for the first time, that the GCMF and GCLF are approximately constant for  $M \lesssim 10^5 M_\odot$  and  $L \lesssim 10^5 L_\odot$ , in stark contradiction to the then-standard practice of fitting log-normal distributions to the data. This behavior of the GCMF at small  $M$  and GCLF at small  $L$  is strong evidence for the late disruption of clusters by internal two-body relaxation. Furthermore, Goudfrooij et al. (2004, 2007) showed that the predicted time dependence of the FZ01 model is consistent with the observed luminosity

functions of intermediate-age (3–4 Gyr old) cluster systems, and Chandar et al. (2007), McLaughlin & Fall (2008), and Goudfrooij (2012) showed that the predicted density dependence agrees well with the observed mass function for subsamples of clusters defined by different ranges of density.

The approximations in the FZ01 model were made for simplicity and to highlight the main physical processes that shape the GCMF and GCLF. In particular, the adoption of classical evaporation and the neglect of  $M/L$  variations are not essential features of the model. Both approximations were in standard use at the time (2001) to describe the evolution of individual clusters. The novel feature of the FZ01 model was to show how the evolution of the masses of individual clusters could be combined analytically into the evolution of the mass function of a cluster system.

At a higher level of approximation, the stellar escape rate is modified by the fact that some of the stars that are scattered into unbound orbits may be scattered back into bound orbits before they have reached the tidal boundary and escaped from a cluster. In this case, often called “retarded” evaporation, the escape rate has a weak dependence on the crossing time  $t_{\text{cr}}$  in addition to the stronger dependence on the relaxation time  $t_{\text{rlx}}$ . For tidally limited, low-mass clusters (initial masses  $M_0 \lesssim 10^5 M_\odot$ ), the evolution can be approximated by  $dM/dt \propto M/t_{\text{dis}}$  with  $t_{\text{dis}} \propto M^\gamma$  and  $\gamma \approx 0.7$ , rather than  $\gamma = 1$  for classical evaporation (Fukushige & Heggie 2000; Baumgardt 2001; Baumgardt & Makino 2003; Lamers et al. 2010). For high-mass clusters, however, the retarded evaporation rate must approach the classical rate (in the limit  $t_{\text{cr}}/t_{\text{rlx}} \rightarrow 0$ ; see Section 5.1).

Two-body relaxation will also cause low-mass stars within a cluster to gain energy and escape faster than high-mass stars, thus reducing the average  $M/L$  of the remaining stars over and above the fading caused by stellar evolution alone. As a result of this effect, in a coeval population of clusters (such as GCs), there should be a positive correlation between  $M/L$  and the mass or luminosity of clusters, because those that have smaller relaxation times will have lost larger fractions of their initial mass. Such variation in  $M/L$  was neglected in the FZ01 model for two reasons: it is difficult to predict reliably from theory, and it appeared from observations at the time to be weak or non-existent (McLaughlin 2000).

Krujsssen & Portegies Zwart (2009, hereafter KPZ09) modified the FZ01 model to include retarded evaporation and a variable  $M/L$  ratio. In particular, they assumed that the rate of mass loss from clusters is given by  $dM/dt \propto M/t_{\text{dis}}$  with  $t_{\text{dis}} \propto M^\gamma$  and  $\gamma = 0.7$  for clusters of all masses. Furthermore, to calculate the escape rates of stars of different masses and hence the variation in  $M/L$  of clusters, they employed a semi-analytical model developed by Krujsssen (2009, hereafter K09) that includes several questionable assumptions and parameter choices. KPZ09 argued that their model is a significant improvement on the FZ01 model, both in terms of its theoretical validity and in terms of its ability to fit the observed GCLF in the Milky Way and other galaxies.

Our main purpose in this paper is to demonstrate that the KPZ09 criticisms of the FZ01 model are not correct. Thus motivated, we also show that the variation in  $M/L$  with  $M$  or  $L$  predicted by the KPZ09 model is much stronger than that allowed by observations. Furthermore, we show that the parameter values required for the KPZ09 model to fit the observed GCLF and the observed  $M/L$  vs.  $L$  relation are mutually exclusive. We emphasize that we do not dispute the general

physical principles underlying retarded evaporation and  $M/L$  variations. The results of this paper indicate, however, that the specific implementation of these effects in the KPZ09 model exaggerates their importance. We find that retarded evaporation and  $M/L$  variations can be neglected for clusters massive enough to survive for a Hubble time of dynamical evolution. Therefore, for most practical purposes, the benefits of including these effects are largely offset by the increased complexity of the KPZ09 model relative to the FZ01 model.

This paper is organized as follows. In Section 2, we compare the FZ01 and KPZ09 models with the observed GCLF in the Milky Way, and we determine the best-fitting values of their parameters including the characteristic dissolution timescale. Section 3 presents our search for  $M/L$  variations of the kind predicted by the KPZ09 model in a large compilation of recent dynamical measurements of GC masses. In Section 4, we compare the dissolution timescale required by the KPZ09 model to match the observed GCLF with the one required by the absence of observed  $M/L$  variations. Section 5 interprets the results from Sections 3 and 4 along with the observed stellar mass functions in Galactic GCs in terms of key properties and assumptions of the K09 model. Finally, we summarize our conclusions in Section 6.

## 2. COMPARISONS OF MODELS WITH THE OBSERVED GCLF

In this Section, we compare the FZ01 and KPZ09 models with the observed GCLF in the Milky Way. We first derive analytical expressions for the evolving GCMFs assuming that the clusters are tidally limited and that stellar escape driven by two-body relaxation is the primary disruption mechanism. We then convert these GCMFs at an age of 12 Gyr into GCLFs adopting  $M/L = \text{constant}$  for the FZ01 model and the  $M/L$  vs.  $L$  relation derived by KPZ09 for their model.

### 2.1. Derivation of Model GCMFs

In both models considered here, the mass-loss rate of an individual cluster takes the form

$$dM/dt \equiv -M/t_{\text{dis}} = -(\mu/\gamma)M^{1-\gamma}, \quad (1)$$

where  $t_{\text{dis}}$  is the dissolution timescale and  $\mu$  and  $\gamma$  are constants. This integrates to

$$M(t) = (M_0^\gamma - \mu t)^{1/\gamma}, \quad (2)$$

where  $M_0$  is the initial cluster mass. These formulae are intended to represent smooth averages over the abrupt changes in mass caused by the escape of individual stars and over at least one full orbit of the cluster around its host galaxy. For  $\gamma = 1$ , equation (1) describes the classical mass-loss rate  $\mu$  for stellar escape driven by internal two-body relaxation from a tidally limited cluster (Spitzer 1987 and references therein). This is the formula adopted in the FZ01 model. For  $\gamma < 1$ , equation (1) approximates the corresponding mass-loss rate for retarded evaporation in relatively low-mass clusters for which crossing times are significant fractions of relaxation times (Fukushige & Heggie 2000; Baumgardt & Makino 2003). The KPZ09 model assumes  $\gamma = 0.7$  for clusters of all masses.

FZ01 showed that the evolution of the mass function  $\psi(M, t)$  of a cluster system could be derived from the evolution of the masses  $M(t)$  of individual clusters through a continuity equation. This approach yields

$$\psi(M, t) = \left(\partial M_0 / \partial M\right)_t \psi_0(M_0) = (M/M_0)^{\gamma-1} \psi_0(M_0), \quad (3)$$

where  $\psi(M_0) = \psi(M_0, 0)$  is the initial mass function (at  $t = 0$ ). In this expression, the initial mass  $M_0$  must be regarded as a function of the current mass  $M$  and current time  $t$  as given by inverting equation (2). Following FZ01, we adopt a Schechter (1976) initial mass function

$$\psi_0(M_0) = A M_0^\beta \exp(-M_0/M_c), \quad (4)$$

with adjustable parameters  $A$ ,  $\beta$ , and  $M_c$ . This function has a power-law shape with exponent  $\beta$  below the bend at  $M_c$  to mimic the observed mass functions of young cluster systems, and it has an exponential decline above  $M_c$  as suggested by the observed tail of the GCMF at  $M \gtrsim 10^6 M_\odot$ . Inserting equation (4) into equation (3) then yields the evolving GCMF:

$$\psi(M, t) = A M^{\gamma-1} (M^\gamma + \mu t)^{(\beta-\gamma+1)/\gamma} \times \exp\left[-(M^\gamma + \mu t)^{1/\gamma}/M_c\right]. \quad (5)$$

This function has a bend at  $M \sim (\mu t)^{1/\gamma}$ ; for lower  $M$ , it behaves as  $\psi(M, t) \propto M^{\gamma-1}$ , characteristic of dissolution by two-body relaxation, while for higher  $M$ , it behaves as  $\psi(M, t) \propto M^\beta \exp(-M/M_c)$ , independent of  $\gamma$ . Thus, we expect only minor differences in the shapes of the GCMF between  $\gamma = 1$  (FZ01 model) and  $\gamma = 0.7$  (KPZ09 model).

The GCMF derived above is strictly valid only in the idealized case that all clusters in the GC system dissolve at the same rate  $\mu$ . In reality, clusters with different internal densities, determined mainly by the galactic tidal field, will dissolve at different rates  $\mu_i$ . In that case, equation (5) can be re-interpreted as the probability density that an individual cluster with evaporation rate  $\mu$  has a mass  $M$  at an age  $t$ . The GCMF of a system of  $\mathcal{N}$  coeval clusters is then the sum of the individual probability densities:

$$\psi(M, t) = \sum_{i=1}^{\mathcal{N}} A_i M^{\gamma-1} (M^\gamma + \mu_i t)^{(\beta-\gamma+1)/\gamma} \times \exp\left[-(M^\gamma + \mu_i t)^{1/\gamma}/M_c\right]. \quad (6)$$

Here  $\beta$  and  $M_c$  are assumed to be the same for all clusters in the GC system, and the normalization factors  $A_i$  must be chosen such that the integral over all  $M$  is unity for each term in the sum.

We now relate the evaporation rate  $\mu$  of a cluster to its mean density  $\rho_h$  within the half-mass radius  $r_h$  as follows. The  $N$ -body simulations of Baumgardt (2001) and Baumgardt & Makino (2003, hereafter BM03) showed that the dissolution time  $t_{\text{dis}}$  of a tidally limited cluster can be approximated by

$$t_{\text{dis}} \propto t_{\text{rlx}} (t_{\text{cr}}/t_{\text{rlx}})^{1-\gamma} \propto M^\gamma \rho_h^{-1/2}, \quad (7)$$

where  $t_{\text{rlx}} \propto M^{1/2} r_h^{3/2}$  is the half-mass relaxation time and  $t_{\text{cr}} \propto M^{-1/2} r_h^{3/2}$  is the half-mass crossing time. The parameter  $\gamma < 1$  in equation (7) is the same as that in equations (1)–(6) and measures the deviation of the dissolution time from the formula  $t_{\text{dis}} \propto t_{\text{rlx}}$  for classical evaporation.<sup>1</sup> The extra factor of  $(t_{\text{cr}}/t_{\text{rlx}})^{1-\gamma}$  for retarded evaporation comes about because unbound stars take a finite time, proportional to  $t_{\text{cr}}$ , to cross a

cluster before escaping from it. During that time, some of the unbound stars will be scattered back into bound orbits within the cluster, thus retarding its evaporation. From equations (7) and (1), we obtain

$$\mu \propto M^\gamma / t_{\text{dis}} \propto \rho_h^{1/2}, \quad (8)$$

independent of  $\gamma$  for both classical and retarded evaporation.<sup>2</sup>

The evaporation rate of a cluster can also be expressed in terms of its mean density  $\rho_t$  within the tidal radius  $r_t$ . This density is determined largely by the tidal field at the pericenter  $R_p$  of the orbit of the cluster within its host galaxy:

$\rho_t \propto G^{-1} (V_{c,p}/R_p)^2$ , where  $G$  is the gravitational constant, and  $V_{c,p}$  is the galactic circular velocity at  $R_p$  (King 1962; Innanen et al. 1983). McLaughlin & Fall (2008) showed that, while the densities  $\rho_h$  and  $\rho_t$  of GCs in the Milky Way span four or five orders of magnitude, the quantity  $(\rho_t/\rho_h)^{1/2}$  varies by less than a factor of two. Thus, to a good approximation, we can rewrite equation (8) in the form

$$\mu \propto \rho_t^{1/2} \propto V_{c,p}/R_p. \quad (9)$$

In an idealized static and spherical galactic potential, the pericenters of all orbits remain fixed, and  $\rho_t$  and hence  $\mu$  are constants of motion.

Both FZ01 and KPZ09 computed the evaporation rates of clusters on different orbits from equation (9) and then summed over a realistic distribution of orbits to determine the mass function  $\psi(M, t)$  of a GC system from equation (6) or its integral equivalent. However, as McLaughlin & Fall (2008) pointed out, the only role of the orbits in this calculation is to determine the cluster densities,  $\rho_h$  or  $\rho_t$ , a step that can be eliminated by computing  $\mu$  directly from the observed values of  $\rho_h$  or  $\rho_t$ . Because tidal radii are notoriously uncertain, evaporation rates are much more robust when computed from  $\rho_h$  than from  $\rho_t$ . This is the approach we take in this paper. Another simplification noted by McLaughlin & Fall (2008) is that the mass function  $\psi(M, t)$  of a GC system computed from equation (5) with the median value of  $\mu$  is very similar to that computed from equation (6) with a realistic distribution of  $\mu$  (see also KPZ09). We refer to the former as single- $\mu$  models and the latter as multiple- $\mu$  models. In this paper, we present results for both types of models, confirming their similarity.

The model GCMFs described above assume that evaporation by two-body relaxation is the dominant disruption mechanism. As such, they neglect the effects of stellar evolution and gravitational shocks. Mass loss by stellar evolution is dominated by supernovae and strong winds of massive stars in the first few  $10^8$  years. This material is assumed to escape from clusters of all masses, thus leaving the shape of the GCMF unchanged. Meanwhile, for surviving GCs in the Milky Way, FZ01 showed that mass loss due to gravitational shocks is generally much weaker than that due to two-body relaxation for clusters with masses below the peak of the GCMF (see also Gnedin & Ostriker 1997; Dinescu et al. 1999). Moreover, the rate of mass loss by gravitational shocks depends only on the densities  $\rho_h$  of clusters, not their masses, which preserves the shape of the GCMF in the sense that both  $\psi$  and  $M$  are simply rescaled by time-dependent factors (see FZ01).

<sup>1</sup> BM03 used the notation  $x$  instead of  $\gamma$  in equation (7). The difference between the two is negligible:  $x$  and  $\gamma$  were derived by evaluating  $t_{\text{dis}}$  as functions of  $N$  (number of particles) and the cluster mass  $M$ , respectively (see Lamers et al. 2010).

<sup>2</sup> To avoid confusion, we note that  $\mu_{\text{ev}}$  in McLaughlin & Fall (2008) is related to our  $\mu$  by  $\mu_{\text{ev}} = (\mu/\gamma) M^{1-\gamma}$ .

## 2.2. Fits of Model GCLFs to Observations

Fitting equation (5) to the observed Galactic GCLF requires a conversion from luminosity to mass. For the FZ01 model ( $\gamma = 1$ ), we simply adopt a mass-independent  $M/L_V$  ratio. For the KPZ09 model ( $\gamma = 0.7$ ), we use their relation between  $M/L_V$  and  $L_V$  at an age of 12 Gyr.<sup>3</sup> The corresponding parameters of the KPZ09 model are: King (1966) concentration parameter  $W_0 = 7$  (the median value of  $W_0$  for the Milky Way GC system, Harris 1996), metallicity  $Z = 0.0004$ , and  $t_0 = 1.3$  Myr. The last of these parameters is defined in the KPZ09 model as  $t_0 \equiv t_{\text{dis}} (M/M_\odot)^{-\gamma}$ , i.e., the dissolution timescale for a cluster with  $M = 1 M_\odot$ . The conversion to our notation is  $t_0 = \gamma/\mu$  (see equation 1).

We derive the observed GCLF of the Milky Way from the 2010 version of the Harris (1996) catalog of GC data. To avoid uncertain luminosities, we exclude 17 GCs with  $E_{B-V} > 1.5$ , resulting in a catalog with 140 GCs.  $V$ -band luminosities are derived by assuming the standard Galactic reddening law (with  $A_V = 3.1 E_{B-V}$ ) and a solar absolute  $V$ -band magnitude of  $M_V^0 = 4.83$  (Binney & Merrifield 1998).

For the single- $\mu$  case, we perform least-squares fits of the model GCLFs to the observed Galactic GCLF using the non-linear Marquardt-Levenberg algorithm (Levenberg 1944; Marquardt 1963). This is done for  $\gamma = 1$  to represent the FZ01 model and for  $\gamma = 0.7$  to represent the KPZ09 model. We adopt  $\beta = -2$ , as found in several studies of young star cluster systems (Fall & Chandar 2012 and references therein). Table 1 lists the reduced  $\chi^2$  values of the two model fits along with the resulting values of the evaporation rate  $\mu$  and the cut-off and peak luminosities,  $L_c$  and  $L_p$ , of the GCLF. Values for  $L_p$  were derived using equation (7) of Goudfrooij (2012).

**Table 1**  
Fits of Single- $\mu$  Models to Galactic GCLF.

Model (1)	$\log L_p/L_{V,\odot}$ (2)	$\log L_c/L_{V,\odot}$ (3)	$(\mu t)^{1/\gamma}$ (4)	rms (5)	$\chi_{\text{red}}^2$ (6)
FZ01	$5.24 \pm 0.04$	$7.15 \pm 0.05$	$(1.80 \pm 0.03) 10^5 \times \Upsilon_V$	0.25	0.68
K09	$5.25 \pm 0.03$	$7.21 \pm 0.04$	$(4.94 \pm 0.05) 10^5$	0.21	0.60
Gaussian	$5.24 \pm 0.04$	N/A	N/A	0.80	5.14

**Note.** — Column (1): model being fit to GCLF. (2): log of turnover luminosity in solar units. (3): log of Schechter cutoff luminosity in solar units. (4): value of  $(\mu t)^{1/\gamma}$  in  $M_\odot$  ( $\Upsilon_V \equiv M/L_V$ ). (5): rms of residuals of fit to GCLF. (6): reduced  $\chi^2$  value of fit to GCLF. See the discussion in § 2.

We also made fits to the observed GCLF derived from the 2003 version of the Harris catalog as a check for consistency with KPZ09 and to estimate the magnitude of systematic errors in the fitted parameter values. We find that the values for both  $\mu t$  and  $L_p$  agree to within 0.5% between the two versions of the Harris catalog, while the values for  $L_c$  come out  $\sim 30\%$  lower for the 2003 version. These differences do not affect any of our conclusions.

For  $M/L_V = 1.8$ , which is the overall mean value found from dynamical data in Sect. 3 below, the evaporation rates of the best-fitting single- $\mu$  FZ01 and KPZ09 models match each other within only 6% at  $\mu \sim 2.6 \times 10^4 M_\odot \text{ Gyr}^{-1}$ . As discussed in detail in McLaughlin & Fall (2008), the corresponding value of  $t_{\text{dis}}/t_{\text{rlx}} \sim 10 (-\beta - 1)^{-1} \sim 10$  where  $\beta$  is the power-

law slope in equation (4).<sup>4</sup> This value of  $t_{\text{dis}}/t_{\text{rlx}}$  is at the low end of the range typically found in theoretical calculations of single-mass clusters ( $t_{\text{dis}}/t_{\text{rlx}} \sim 10-40$ ). However, simulations of multi-mass clusters have shown evaporation rates that are significantly larger than those of single-mass clusters (e.g., Lee & Goodman 1995). Furthermore, evaporation rates depend on the specific techniques, assumptions, and approximations used for each simulation (see, e.g., Gnedin & Ostriker 1997; Vesperini & Heggie 1997; Baumgardt & Makino 2003; Prieto & Gnedin 2008; Heggie 2014).

For the multiple- $\mu$  case, we proceed as follows. We compute FZ01 and KPZ09 models from equation (6), adopting the values of  $M_c$  listed in Table 1 along with  $\beta = -2$  as before. To compute the evaporation rates  $\mu_i$  of individual clusters, we again assume an age  $t = 12$  Gyr, and we use the values of  $\mu t$  in Table 1 for a cluster with the median density  $\hat{\rho}_h$ . We then use the current half-mass density of each Galactic GC to estimate its evaporation rate from  $\mu_i = (\rho_{h,i}/\hat{\rho}_h)^{1/2}$  (see equation 8). Again, we adopt the 2010 version of the Harris (1996) catalog,  $M/L_V = 1.8$  for  $\gamma = 1.0$  (i.e., the FZ01 model), and the KPZ09 relation between  $M/L_V$  and  $L_V$  for  $\gamma = 0.7$ .

The resulting FZ01 and KPZ09 models are compared with the observed GCLF in Fig. 1. Panels (a) and (c) show the GCLF in the form  $dN/d \log L = (L \ln 10) dN/dL$  vs.  $\log L$ , analogous to the familiar observed GCLFs in magnitude space, whereas panels (b) and (d) show the GCLF in the form  $\log(dN/dL)$  vs.  $\log L$ . For comparison with the more traditional log-normal representation of the GCLF, we also overplot a best-fit Gaussian whose parameters are  $(\log(L_V/L_{V,\odot})) = 5.24 \pm 0.04$  and  $\sigma_{\log L} = 0.64 \pm 0.05$  in panels (a) and (b).

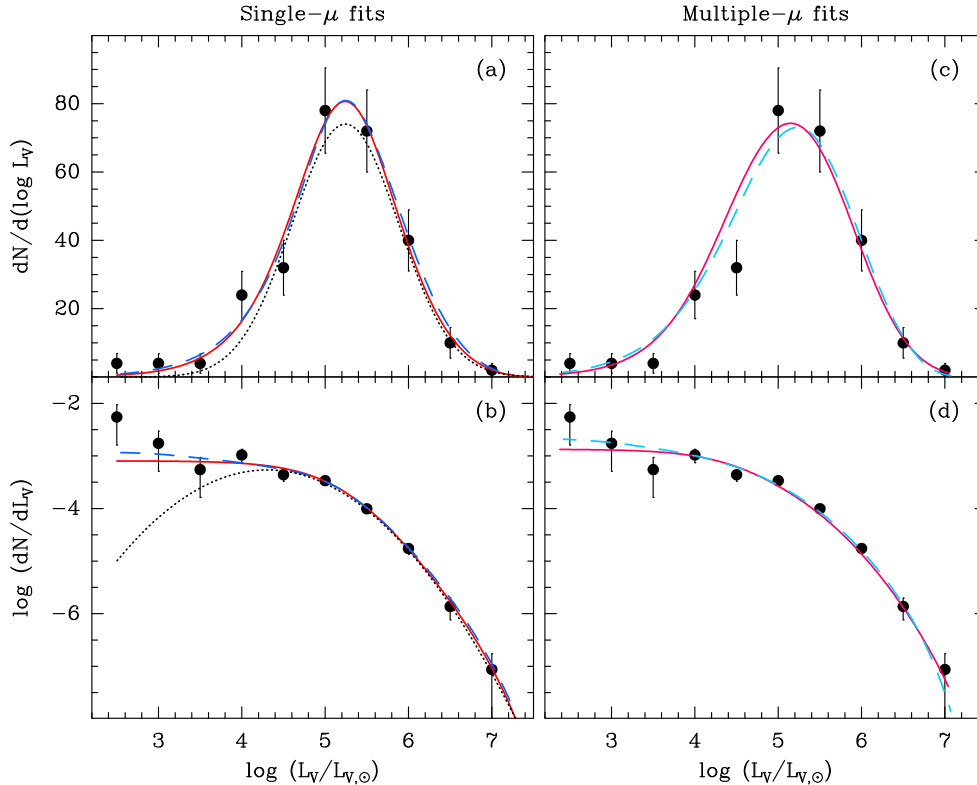
As Fig. 1 shows, the differences between the FZ01 and KPZ09 models in their ability to fit the observed GCLF are very small relative to the uncertainties. This holds for both the single- $\mu$  and multiple- $\mu$  models. Statistically, the KPZ09 model fits the data slightly better at  $\log(L_V/L_{V,\odot}) \lesssim 3.5$ , while the FZ01 model fits better at  $L \gtrsim L_p$ . However, we emphasize that these differences are negligible not only with respect to the poisson errors, but also when compared to the improvement that the FZ01 and KPZ09 models provide over the traditional Gaussian representation of the GCLF. This is due to the asymmetry in the observed GCLF in that there are more GCs at  $L < L_p$  than at  $L > L_p$ . This asymmetry is especially clear in panels (b) and (d) of Fig. 1 which show that  $\psi(L) = dN/dL$  is approximately flat for GCs with  $L_V \lesssim 10^4 L_{V,\odot}$ . This behavior is clearly not consistent with a Gaussian LF, while it is matched very well by both the FZ01 and the KPZ09 models.

Fig. 1 also shows that there is no significant difference between the single- $\mu$  and multiple- $\mu$  models in terms of fitting the observed GCLFs, confirming the findings of FZ01 and KPZ09. Quantitatively, the reduced  $\chi^2$  values of the multiple- $\mu$  fits are 0.61 and 0.59 for the FZ01 and KPZ09 models, respectively. In the remainder of this paper, we adopt the single- $\mu$  models for simplicity.

It is worth noting that the GCLFs of the FZ01 and KPZ09 models are more similar than are their GCMFs (see Fig. 1 of KPZ09). The reason for this is that the different relations between  $M/L_V$  and  $L_V$  largely compensate for the differences in the GCMFs. We conclude that the shape of the Galactic GCLF does not provide any evidence for a GC mass-

<sup>3</sup> This relation was shown in Fig. 4 of KPZ09, and with more clarity, in Krujijssen & Portegies Zwart (2010).

<sup>4</sup> Note that  $\beta$  in this paper is equal to  $-\beta$  in McLaughlin & Fall (2008).



**Figure 1.** *Panel (a):* Fits of the single- $\mu$  FZ01 model (red solid curve), the single- $\mu$  KPZ09 model (blue dashed curve), and a Gaussian (black dotted curve) to the Galactic GCLF, expressed as the number of GCs per unit logarithm of  $V$ -band luminosity. *Panel (b):* Similar to panel (a), but now in terms of  $\log(dN/dL_V)$  vs.  $\log L_V$ . *Panel (c):* Similar to panel (a), but now for the multiple- $\mu$  models described in the text. The light red solid curve represents the FZ01 model while the light blue dashed curve represents the KPZ09 model. *Panel (d):* Similar to panel (c), but now in terms of  $\log(dN/dL_V)$  vs.  $\log L_V$ . All models are drawn for an age of 12 Gyr.

dependent  $M/L_V$  ratio. Thus, the claim by KPZ09 that “the match between the models and the observations [of the Galactic GCLF] exists only for values of  $\gamma \approx 0.7$ ” is not correct.

### 3. SEARCHES FOR DYNAMICAL $M/L$ VARIATIONS

The most reliable estimates of GC masses are those derived from stellar kinematics, often referred to as “dynamical masses”. KPZ09 argued that the dependence of  $M/L$  on  $L$  predicted by their model was supported by the dynamical masses compiled by Mandushev et al. (1991) who found a weak correlation between  $M/L$  and  $M$  due to a few high  $M/L$  values at  $\log(M/M_\odot) \gtrsim 5.5$ . However, no such correlation appears in the more homogeneous and larger compilation of  $M/L$  values by McLaughlin (2000), which superseded most of the Mandushev et al. results. With this in mind, we review recent measurements of dynamical  $M/L$  ratios of ancient GCs in the literature to search for any dependence on GC luminosity similar to that predicted by the KPZ09 model. We test for a dependence of  $M/L$  on GC luminosity rather than GC mass because the uncertainties in GC luminosities are typically relatively small and similar among clusters. In contrast, the uncertainties in GC masses vary significantly among clusters, depending on measurement specifics (e.g., numbers of stars measured, radial coverage). Thus, the correlation between measurement errors of  $M/L$  and  $\log L$  is much smaller than between those of  $M/L$  and  $\log M$ .

We include measurements from five independent studies of Galactic GCs: McLaughlin & van der Marel (2005, 37 GCs), Lützgendorf et al. (2013, 14 GCs), Zaritsky et al. (2012, 2013, 2014, 14 GCs), Kimmig et al. (2015, 25 GCs), and Watkins et al. (2015, 15 GCs). In addition, we use the

large sample of 178 old GCs in the Andromeda galaxy by Strader et al. (2011).

#### 3.1. Limits on $M/L_V$ Variations in Milky Way GCs

The dynamical  $M/L_V$  measurements of the five samples of Galactic GCs are shown as a function of  $\log L_V$  in panels (a)–(e) of Fig. 2. For each cluster sample, the overall average value of  $M/L_V$  is shown by a horizontal dashed line. For comparison with the predictions of the KPZ09 model, we also overplot their relation between  $M/L_V$  and  $L_V$  at an age of 12 Gyr.

Systematic differences among dynamical  $M/L_V$  values derived by the five studies mentioned above are described in detail in the Appendix. Panel (f) of Fig. 2 shows our correction for these systematic differences, which are mainly due to the different ways to convert observed  $M/L_V$  to “global” values that apply to each cluster as a whole. We adopt the normalization of Lützgendorf et al. (2013). Thus, we multiply the  $M/L_V$  values of McLaughlin & van der Marel (2005), Zaritsky et al. (2012, 2013, 2014), Kimmig et al. (2015), and Watkins et al. (2015) by factors of 1.20, 1.75, 1.26, and 1.07, respectively (see Appendix A).

As Fig. 2 clearly shows, there is no evidence favoring the relation between  $M/L_V$  and  $L_V$  in the KPZ09 model over the constant  $M/L_V$  ratio in the FZ01 model. This is quantified in Table 2, which lists the  $\chi^2$  values of the fits for the two models to the five data samples shown in Fig. 2.<sup>5</sup> Specifically, the mass-independent  $M/L_V$  model yields somewhat

<sup>5</sup> The fits of the KPZ09 model to the data were performed by allowing for a  $L_V$ -independent scale factor in  $M/L_V$ .

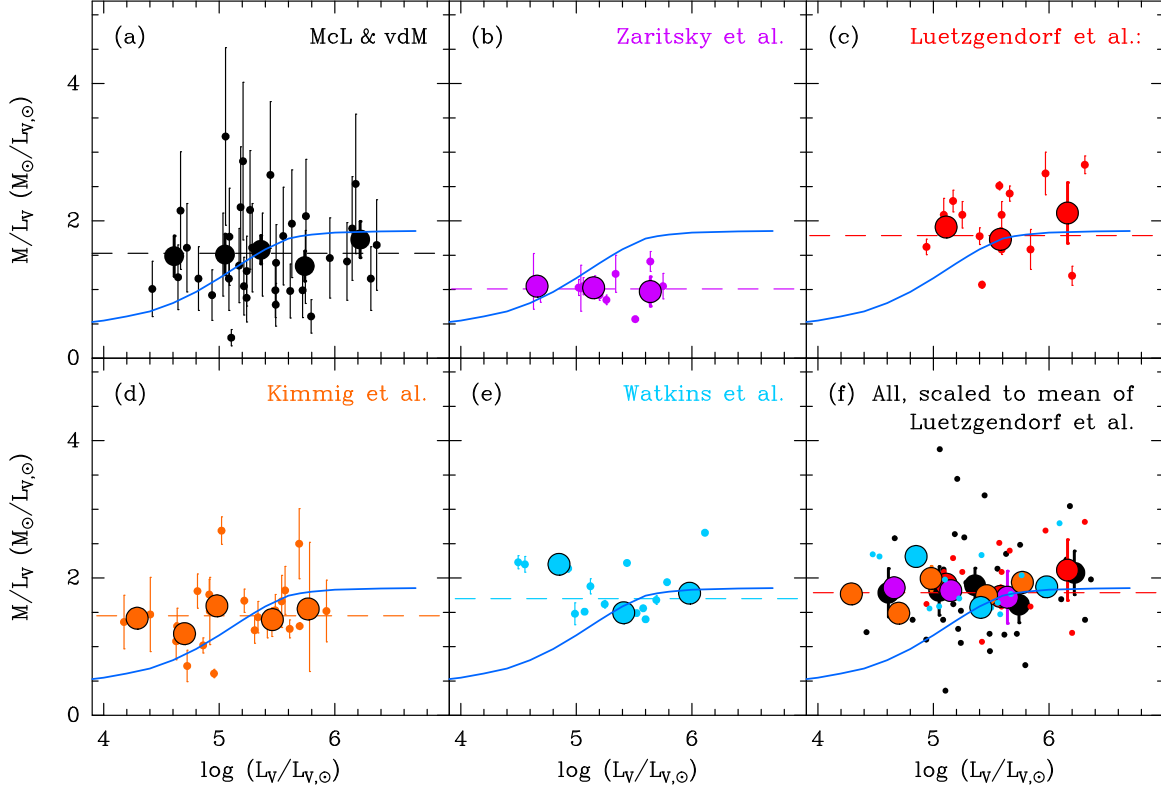


**Figure 2.** *Panel (a):* observed dynamical  $M/L_V$  ratios of Galactic GCs from McLaughlin & van der Marel (2005, black circles) as a function of their  $V$ -band luminosities. The large filled circles depict average values in five bins of equal size in  $\log(L_V/L_{V,\odot})$ . For comparison, we overplot the overall average value of  $M/L_V$  (dashed line) and the relation between  $M/L_V$  and  $\log(L_V/L_{V,\odot})$  at an age of 12 Gyr predicted by the KPZ09 model (blue solid line). *Panel (b):* similar to panel (a), but now showing data from Zaritsky et al. (2012, 2013, 2014), purple circles). *Panel (c):* similar to panel (a), but now showing data from Lützgendorf et al. (2013, red circles). *Panel (d):* similar to panel (a), but now showing data from Kimmig et al. (2015, orange circles). *Panel (e):* similar to panel (a), but now showing data from Watkins et al. (2015, light blue circles). *Panel (f):* a combination of all  $M/L_V$  ratios from the five studies depicted in panels (a)–(e), after correcting for systematic differences between the mean  $M/L_V$  values of the individual studies (see text in Sect. 3.1.1). For clarity, the data for the individual GCs in panel (f) are shown without errorbars.

**Table 2**  
Fits of Models to Observed Dynamical  $M/L_V$  Values.

Parameter (1)	McL & vdM		Lützgendorf		Zaritsky		Kimmig		Watkins		Strader	
	FZ01 (2)	K09 (3)	FZ01 (4)	K09 (5)	FZ01 (6)	K09 (7)	FZ01 (8)	K09 (9)	FZ01 (10)	K09 (11)	FZ01 (12)	K09 (13)
$\sigma/\sqrt{N}$	0.73	0.81	0.57	0.61	0.27	0.49	0.56	0.72	0.41	0.71	0.70	0.79
$\chi^2_{\text{red}}$	0.38	0.49	0.29	0.32	0.04	0.10	0.21	0.33	0.15	0.41	0.40	0.50
$ \langle \Delta\chi^2_{\text{red}} \rangle $	0.12		0.04		0.06		0.11		0.11		0.08	
$\sigma( \Delta\chi^2_{\text{red}} )$	0.08		0.05		0.05		0.06		0.03		0.04	

**Note.** — Column (1): parameter name (standard error, reduced  $\chi^2$ , absolute mean value of  $\Delta\chi^2_{\text{red}}$ , and standard deviation of  $|\Delta\chi^2_{\text{red}}|$ ). See the discussion in § 3.1 for the meaning of the latter two parameters. Columns (2) and (3): values for FZ01 and K09 model fits to McLaughlin & van der Marel (2005) data, respectively. Columns (4) and (5): same as columns (2) and (3), respectively, but now for Lützgendorf et al. (2013) data. Columns (6) and (7): same as columns (2) and (3), respectively, but now for Zaritsky et al. (2012, 2013, 2014) data. Columns (8) and (9): same as columns (2) and (3), respectively, but now for Kimmig et al. (2015) data. Columns (10) and (11): same as columns (2) and (3), respectively, but now for Watkins et al. (2015) data. Columns (12) and (13): same as columns (2) and (3), respectively, but now for Strader et al. (2011) data.

better fits to the data of McLaughlin & van der Marel (2005), Zaritsky et al. (2012, 2013, 2014), Kimmig et al. (2015), and, more clearly, to the data of Watkins et al. (2015).

To put the  $\chi^2$  values in Table 2 in context, we performed a series of Monte Carlo simulations as follows. For each of the five  $M/L$  datasets with individual luminosities  $L_i$ , we calculate masses  $M_i$  under the assumptions of both the FZ01 model (using a constant  $M/L_V = 1.8$ ) and the KPZ09 model (using their  $M/L_V$  vs.  $L_V$  relation). To each of the  $L_i$  and  $M_i$  values we then add random measurement errors based on

the distribution of such errors in the dataset in question. The synthetic  $M_i/L_i$  data that are intrinsically distributed like the FZ01 model are then fitted by the KPZ09 model, and vice versa. We define  $\Delta\chi^2_{\text{red}} \equiv \chi^2_{\text{red, KPZ09}} - \chi^2_{\text{red, FZ01}}$ , i.e., the difference in  $\chi^2_{\text{red}}$  between the KPZ09 and FZ01 model fits. These simulations were performed 1000 times for each of the five datasets. The resulting distributions of  $\Delta\chi^2_{\text{red}}$  thus reflect the expected probabilities to find a given difference in  $\chi^2_{\text{red}}$  between the two model fits for the dataset in question.

Fig. 3 shows the distributions of  $\Delta\chi_{\text{red}}^2$ , while Table 2 lists the corresponding absolute mean values  $|\langle\Delta\chi_{\text{red}}^2\rangle|$  and standard deviations  $\sigma(|\Delta\chi_{\text{red}}^2|)$ . Comparing the values of  $\langle\Delta\chi_{\text{red}}^2\rangle$  with the measured differences in  $\chi_{\text{red}}^2$  between the KPZ09 and FZ01 fits to the five  $M/L$  datasets (which are shown in Fig. 3 as vertical arrows), we find that the measured differences in  $\chi_{\text{red}}^2$  are all consistent with the hypothesis that a constant  $M/L$  fits the data better than the KPZ09 model. Quantitatively, the KPZ09 model is excluded by the data at confidence levels of  $2.9\sigma$ ,  $1.4\sigma$ ,  $2.4\sigma$ ,  $3.8\sigma$ , and  $12.3\sigma$ , for the datasets of McLaughlin & van der Marel, Lützgendorf et al., Zaritsky et al., Kimmig et al., and Watkins et al., respectively.

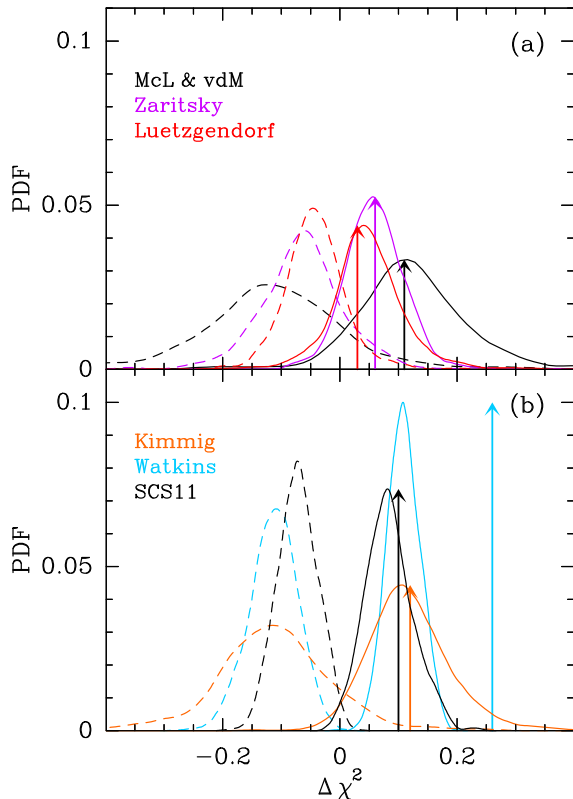


**Figure 3.** Panel (a): probability densities of  $\Delta\chi_{\text{red}}^2$  values (see Sect. 3.1 for its definition) for the  $M/L_V$  datasets shown in Figs. 2 and 5: McLaughlin & van der Marel (2005, black line), Zaritsky et al. (2012, 2013, 2014, purple line), and Lützgendorf et al. (2013, red line). For all datasets, the solid and dashed curves represent sets of Monte-Carlo simulations in which the  $M/L_V$  values of GCs are intrinsically distributed according to the FZ01 and KPZ09 models, respectively. For comparison, the measured differences in  $\chi_{\text{red}}^2$  between the KPZ09 and FZ01 model fits to the  $M/L_V$  values of those datasets are shown by vertical solid arrows in the color of the dataset in question. Panel (b): similar to panel (a), but now for the datasets of Kimmig et al. (2015, orange line), Watkins et al. (2015, light blue line), and SCS11 (black line; see Sect. 3.2).

We also note the lack of a correlation between dynamical  $M/L_V$  and metallicity  $[\text{Fe}/\text{H}]$  at any GC luminosity in Figure 4. This is not consistent with the relation predicted by simple stellar population (SSP) models, as illustrated by the solid line in Fig. 4. This suggests that the  $M/L_V$  values of ancient GCs are more affected by their dynamical histories than by their metallicities.<sup>6</sup> For multi-mass King models of stellar

systems, Shanahan & Gieles (2015) showed that the lack of correlation between  $M/L_V$  and  $[\text{Fe}/\text{H}]$  among GCs can be explained by mass segregation, which causes the brighter, more massive stars in the central regions, where the kinematic measurements are typically made, to move with lower velocities than the fainter, less massive stars in the outskirts, and whose effect is stronger at higher metallicities due to the increasing turn-off mass with higher metallicity.

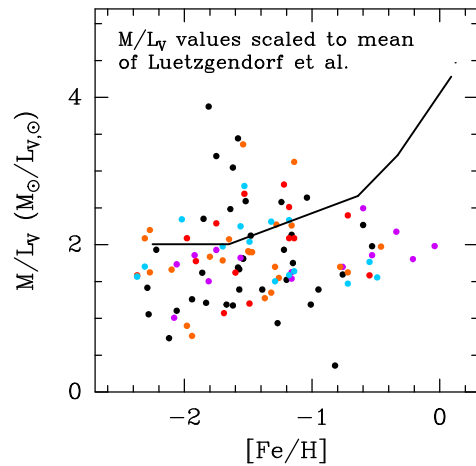


**Figure 4.** Measured  $M/L_V$  values of Galactic GCs shown in panel (f) of Fig. 2 versus  $[\text{Fe}/\text{H}]$ . Symbol colors are the same as in Fig. 2. For comparison, the solid line represents the SSP model predictions of Bruzual & Charlot (2003) for a Chabrier (2003) IMF.

The effect of stellar mass segregation on dynamical mass measurements is also mass-dependent, since present-day low-mass clusters have survived many more relaxation times on average than high-mass clusters. This means that the current level of mass segregation increases with decreasing GC mass, which causes dynamical masses of GCs to be *systematically underestimated for low-mass GCs*.<sup>7</sup> This reinforces our conclusion that the dynamical  $M/L_V$  data show no evidence for the  $M/L_V$  variations predicted by the KPZ09 model.

### 3.2. Limits on $M/L_V$ Variations in Andromeda GCs

We can also compare the model  $M/L$  ratios to the observed ones for GCs in the Andromeda galaxy (M31). Strader et al. (2011, hereafter SCS11) derived dynamical  $M/L$  ratios for a large sample ( $N = 178$ ) of old GCs in M31, covering a wide range of luminosities ( $4.7 \lesssim \log(L_V/L_{V,\odot}) \lesssim 6.5$ ). We adopt the GC masses that they derived using the virial theorem, as well as their  $V$ -band luminosities. We also follow SCS11 in discarding GCs whose relative errors in  $M/L_V$  are larger than 25%.

To evaluate the luminosity dependence of the  $M/L_V$  ratio from the M31 data, we first consider a subselection in metallicity. As reported by SCS11, the  $M/L$  ratios of their metal-rich GCs ( $[\text{Fe}/\text{H}] \gtrsim -0.5$ ) are systematically and significantly lower than that of SSP model predictions. This contrasts with the lower-metallicity GCs whose  $M/L_V$  ratios scatter around the SSP model predictions (cf. Fig. 1 of SCS11). As mentioned in the previous subsection, this behavior is consistent with mass segregation, whose effect is especially strong at  $[\text{Fe}/\text{H}] > -0.5$  (Shanahan & Gieles 2015). To minimize the

<sup>6</sup> This also explains why one can safely neglect the metallicity dependence of  $M/L$  when fitting the GCLF by cluster evolution models as in Sect. 2 (see also FZ01 and KPZ09).

<sup>7</sup> This trend might not extend to the lowest-mass clusters ( $\log(M/M_\odot) \lesssim 4.5$ ) which have only  $\lesssim 10\%$  of their lifetimes remaining and may already have undergone core collapse (see, e.g., BM03).

bias introduced by mass segregation (i.e., causing underestimates of  $M/L$  whose amplitude is mass-dependent), we therefore subselect GCs with  $[\text{Fe}/\text{H}] < -0.5$ .

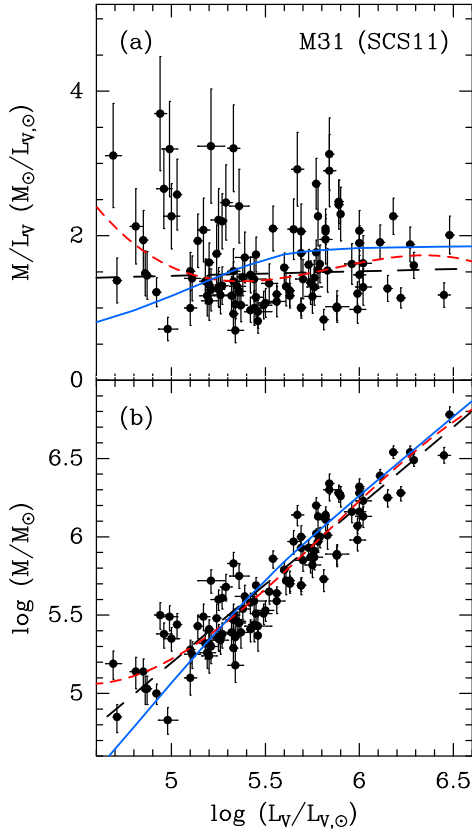


**Figure 5.** Panel (a): dynamical  $M/L_V$  versus  $\log L_V$  for the sample of GCs in the Andromeda galaxy (M31) from SCS11. For comparison, we overplot linear and cubic fits to the data (long-dashed and short-dashed lines, respectively) and the relation between  $M/L_V$  and  $\log L_V$  predicted by the KPZ09 model for an age of 12 Gyr (solid line). Panel (b): similar to panel (a), but now for  $\log M$  versus  $\log L_V$ . See the discussion in Sect. 3.2.

Panel (a) of Fig. 5 shows  $M/L_V$  versus  $\log L_V$  for the resulting sample of 109 GCs in M31. Linear and cubic fits to the data (using inverse variance weighting) are shown as black and red dashed lines, respectively, while the prediction of the KPZ09 model is shown as a blue solid line. Overall, the picture is very similar to that for the Galactic GCs in panel (c) of Fig. 2 in that  $M/L_V$  is again independent of  $L_V$ . Quantitatively, the linear fit to the data has a slope  $d(M/L_V)/d(\log L_V) = 0.06 \pm 0.13$ , while the cubic fit actually shows a marginal upturn of  $M/L_V$  at  $\log(L_V/L_{V,\odot}) \lesssim 5.2$ , where the KPZ09 model predicts a downturn.

This result may seem surprising, since SCS11 reported a correlation between  $M/L_V$  and  $\log M$  for the same dataset, similar to that predicted by the KPZ09 model. We find that their apparent correlation results from a strong covariance of  $M/L_V$  and  $\log M$ , due to correlated errors, rather than a true physical relationship.<sup>8</sup> To illustrate this, we also perform linear and cubic fits between the *independent* variables  $\log L_V$  and  $\log M$  for the SCS11 dataset. A glance at panel (b) of Fig. 5 confirms the trends seen in  $M/L_V$  vs.  $L_V$  discussed above. Finally, we calculate  $\chi^2$  values of fits of the two mod-

<sup>8</sup> A similar situation is found for the dataset of Kimmig et al. (2015) discussed in Sect. 3.1.

els (i.e., constant  $M/L$  and the KPZ09 model) to the SCS11 data. These values are listed in Table 2. Similar to our results from the Galactic GC samples, we find that the constant  $M/L$  model provides a better fit to the M31 data than the KPZ09 model. We also performed Monte Carlo simulations like those described in Sect. 3.1 for the SCS11 dataset. The results are listed in Table 2. We find that the KPZ09 model is excluded by the SCS11 data at a confidence level of  $4.5\sigma$ .

We conclude that the available data on dynamical  $M/L_V$  ratios for ancient GCs in the Milky Way and M31 provide no evidence for a dependence on GC luminosity of the kind predicted by the KPZ09 model. Specifically, the decline of  $M/L_V$  with decreasing  $L_V$  below  $\log(L_V/L_{V,\odot}) \approx 5.2$  predicted by the KPZ09 model is not seen in the data.

#### 4. CONSTRAINTS FROM SIMULTANEOUS FITS TO THE GCLF AND THE $M/L_V$ VERSUS $L_V$ RELATION

In this Section, we check whether the discrepancy between the observed  $M/L_V$  data at low GC luminosities and the predictions of the KPZ09 model discussed in Sect. 3.1 may be resolved by increasing the characteristic dissolution timescale  $t_0$ , taking the fit to the GCLF into account as well. To do this, we turn to the full set of K09 models that are available online.<sup>9</sup> In the following, we will refer to the KPZ09 model with  $t_0 = 1.3$  Myr and  $W_0 = 7$  discussed above as the “reference” K09 model.

The impact of higher values of  $t_0$  on the  $M/L_V$  ratios predicted by the K09 models as a function of  $L_V$  is shown in panel (b) of Fig. 6, which is a copy of panel (f) of Fig. 2 to which we have added the K09 model predictions for  $t_0 = 3$  and 10 Myr as dashed and dash-dotted lines, respectively. Note that the K09 models with higher values of  $t_0$  are closer to the observed nearly flat distribution of dynamical  $M/L_V$  data than the reference model with  $t_0 = 1.3$  Myr.

We then calculate the corresponding GCLFs for an age of 12 Gyr predicted by the K09 models for  $t_0 = 3$  and 10 Myr, respectively. To do so, we adopt the same initial GCMF as before, i.e., a Schechter function with  $\beta = -2$  and  $M_c = 9 \times 10^6 M_\odot$  (cf. Sect. 2 and Table 1). The initial GC masses are then converted into masses and  $V$ -band luminosities at an age of 12 Gyr by means of the K09 model tables, using spline interpolation. Finally, present-day GCLFs are calculated from the GCMFs using  $dN/d\log L_V = (dN/d\log M) (d\log M/d\log L_V)$  where  $d\log M/d\log L_V$  represents the local slope of the relation between  $\log L_V$  and  $\log M$  at an age of 12 Gyr in the K09 models. The resulting GCLFs are depicted in panel (a) of Fig. 6. Note that the GCLFs predicted for the K09 models with  $t_0 = 3$  and 10 Myr do not fit the GCLF well at all in that they peak at significantly lower luminosities than do the data and the reference K09 model (with  $t_0 = 1.3$  Myr), due to the lower evaporation rates. We have verified that the K09 model GCLFs for  $t_0 = 3$  and 10 Myr are not sensitive to the adopted cutoff mass  $M_c$  for  $\log(L_V/L_{V,\odot}) \lesssim 6$ , even when  $M_c$  is increased by factors up to  $10^3$ .

We conclude that there is no value of  $t_0$  for the K09 model that is able to fit the GCLF and the  $M/L_V$  data at  $\log(L_V/L_{V,\odot}) \lesssim 5$  simultaneously. In contrast, the lack of a luminosity dependence of  $M/L_V$  seen in panel (b) of Fig. 6 is fitted naturally by the FZ01 model with a constant  $M/L$ .

To check the robustness of this conclusion, we compare the distributions of relative evaporation rates  $\mu$  of the GCs with

<sup>9</sup> The K09 SPACE models are available at <http://bit.ly/1Pbttlg>.



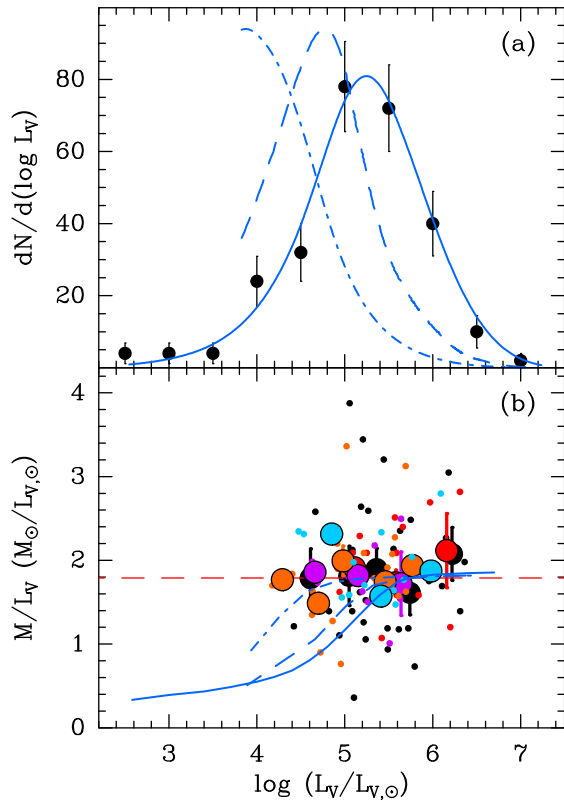


**Figure 6.** *Panel (a):* observed Galactic GCLF compared with the K09 model at an age of 12 Gyr for three values of the dissolution timescale:  $t_0 = 1.3, 3,$  and  $10$  Myr (blue solid, dashed, and dashed-dotted lines, respectively). *Panel (b):* dynamical  $M/L_V$  ratios of Galactic GCs as a function of their  $V$ -band luminosities. This is a copy of panel (f) of Fig. 2, to which we have added K09 model predictions for  $t_0 = 3$  and  $10$  Myr in blue dashed and dash-dotted lines, respectively. See the discussion in Section 4.

$\log(L_V/L_{V,\odot}) \leq 5$  that have dynamical  $M/L_V$  measurements with those of all Milky Way GCs in the same luminosity range (cf. panel (b) of Fig. 6). Once again, we use the 2010 version of the Harris (1996) catalog, using  $M/L = 1.8$  for  $\gamma = 1.0$ , and the KPZ09  $M/L_V$  vs.  $L_V$  relation for  $\gamma = 0.7$  (cf. Section 2.2). This comparison is shown in Fig. 7. Note that the distributions of relative  $\mu$  values of the two samples are very similar to each other, with the median value actually being slightly larger for the sample with dynamical  $M/L_V$  measurements. This holds for both classical and retarded evaporation ( $\gamma = 1.0$  and  $0.7$ ). The inability of the K09 model to fit both the GCLF and the  $M/L_V$  data at low luminosities simultaneously is therefore *not* due to a mismatch between dissolution timescales of the low-luminosity Galactic GCs with available  $M/L_V$  data and those of the full sample of Galactic GCs in the same luminosity range.

## 5. ASSESSING KEY INGREDIENTS OF THE K09 MODEL

In this Section, we assess our findings from the preceding Sections in the context of effects that were neglected in the FZ01 model but included in the K09 model, and which KPZ09 claim are significant improvements.

### 5.1. Mass Dependence of Retarded Evaporation Rates

We recall that the reference K09 model assumes  $\gamma = 0.7$  and  $W_0 = 7$  for clusters of all masses. This choice was based on approximations by Lamers et al. (2010), which in turn were based on the  $N$ -body simulations by BM03 (cf. Sect. 2.1). While retarded evaporation can be expected to occur in all

GCs at some level, it seems unlikely that a single value of  $\gamma$  applies to GCs across the full range of initial masses. Because of the scaling  $t_{\text{cr}}/t_{\text{rlx}} \propto M^{-1}$ , stars that reach escape velocities in high-mass GCs leave the cluster quicker relative to the situation in lower-mass GCs, implying that  $\gamma$  should increase with GC mass. In fact, if a fixed  $\gamma < 1$  applied for all GC masses, one would obtain an unphysical  $t_{\text{dis}} < t_{\text{rlx}}$  at some high GC mass (see also Baumgardt 2001). We therefore expect  $\gamma$  to approach unity for GCs with sufficiently high initial masses.

The expected increase of  $\gamma$  with initial cluster mass  $M_0$  is relevant because Lamers et al. (2010) derived the value  $\gamma = 0.7$  from  $N$ -body simulations by BM03 with  $4 \times 10^3 \lesssim M_0/M_\odot \lesssim 7 \times 10^4$  (corresponding to  $8192 \leq N_0 \leq 131072$  for a Kroupa (2001) IMF). However, the great majority of GCs that survive for a Hubble time were initially much more massive than that. This is illustrated in Fig. 8 which shows the relation between the masses at  $t = 0$  and 12 Gyr computed from equation (2) for  $\gamma = 1.0$  and  $0.7$  with the best-fit values of  $\mu$  from Table 1. For comparison, we also show the same models with evaporation rates that are factors 0.5 and 2.0 times those of the respective best-fit values. Note that the simulated clusters used to derive  $\gamma = 0.7$  by Lamers et al. (2010), which have  $M_0 \leq 10^{4.8} M_\odot$ , do not even survive 12 Gyr of dynamical evolution according to these models. For a moderately low-mass GC with current mass  $M \approx 10^{4.5} M_\odot$  for which the K09 models predict  $M/L_V$  to be about half of that of high-mass GCs (see Sect. 3), the initial mass indicated by these models is in the range  $10^{5.5} - 10^6 M_\odot$ , depending on the model. It is thus clear that *the GCs that currently make up the bulk of the Galactic GC system were initially at least one order of magnitude more massive than the simulated clusters used to derive  $\gamma = 0.7$  by Lamers et al. (2010)*. Since  $\gamma$  is expected to increase with increasing GC mass (cf. above), it seems prudent to regard the value  $\gamma = 0.7$  adopted by K09 as a lower limit.

In summary,  $\gamma$  is expected to increase from  $\approx 0.7$  for low-mass clusters to  $\approx 1.0$  for high-mass clusters. Future  $N$ -body simulations with substantially more particles ( $N$  in the approximate range  $10^{5.5} - 10^{6.5}$  according to Fig. 8) will be needed to determine the actual dependence of  $\gamma$  on initial cluster mass.

### 5.2. Other Assumptions in the K09 Model

The semi-analytical model of K09 involves a large number of other parameters, assumptions, and approximations (in addition to  $\gamma = 0.7$  and  $W_0 = 7$  for the reference K09 model). Some of these ingredients are plausible, but some others are ad hoc and/or not tested against observations, more rigorous theory, or realistic  $N$ -body simulations. Given these uncertain inputs to the model, it seems likely that the outputs from it will also be uncertain. Examples of assumptions in the K09 models whose quantitative effects are hard to estimate include the following.

- The initial-final mass relations for dark remnants (white dwarfs, neutron stars, and stellar-mass black holes).
- The distributions of kick velocities of the various types of dark remnants, and the dependence of the retention fractions of such remnants on (initial) cluster escape velocity.
- The stellar mass dependence of the escape rate, for which the K09 models adopt the Hénon (1969) rate

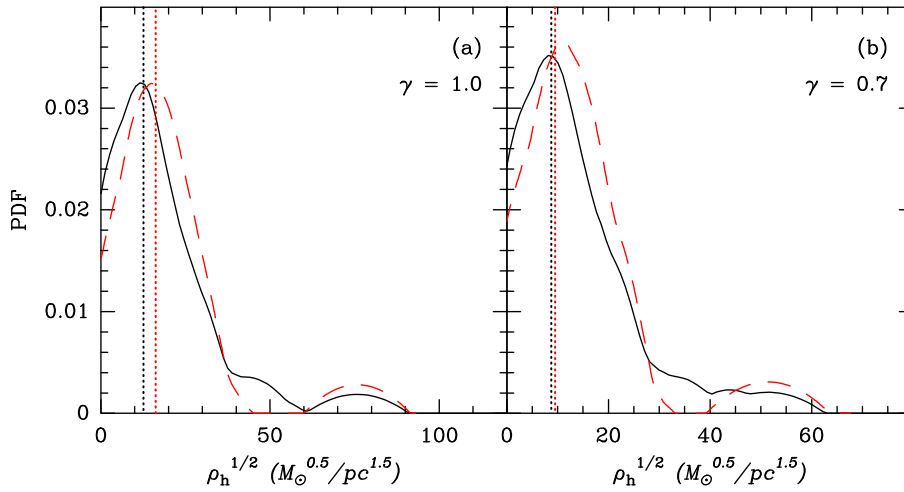


**Figure 7.** Probability densities of relative evaporation rates  $\mu \propto \rho_h^{1/2}$  of Galactic GCs. *Panel (a)*: “classical” evaporation rates (for  $\gamma = 1.0$ ). *Panel (b)*: “retarded” evaporation rates (for  $\gamma = 0.7$ ). In both panels, the black solid line represents all Galactic GCs with  $4.0 < \log(L_V/L_{V,\odot}) < 5.0$ , while the red dashed line represents GCs with  $4.0 < \log(L_V/L_{V,\odot}) < 5.0$  that have dynamical  $M/L$  measurements shown in Figs. 2 and 6. Vertical black and red dotted lines indicate the median values of the respective distributions. See the discussion in Section 4.

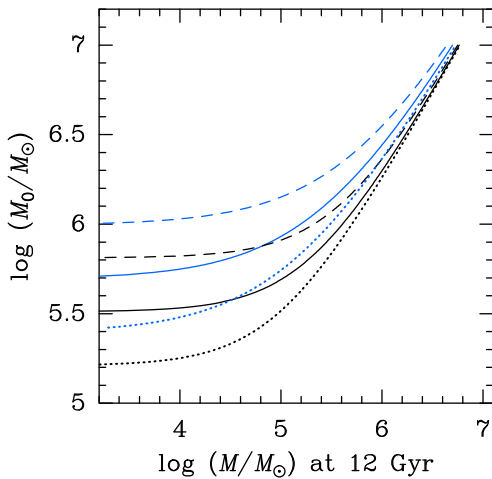


**Figure 8.** Relation between initial GC mass ( $M_0$ ) and GC mass at an age of 12 Gyr ( $M$ ) for different dynamical evolution models. The solid lines show the single- $\mu$  models that fit the Galactic GCLF for  $\gamma = 1.0$  (FZ01 model; black line) and  $\gamma = 0.7$  (KPZ09 model; blue line). The dashed and dotted lines in a given color represent the same models but with evaporation rates that are scaled up and down by a factor 2 relative to the best-fit values, respectively. See the discussion in Section 5.1.

for *close* stellar encounters in an *isolated* cluster (i.e., not residing in a tidal field) without mass segregation. However, real GCs *are* located in a (time-dependent) tidal field and stars escape mainly through repeated *weak* encounters (i.e., two-body relaxation), for which the dependence of the escape rate on stellar mass may be different.

- The assumption of perfect energy equipartition during the mass-segregation phase of dynamical evolution. This assumption, which has an impact on the stellar mass dependence of evaporation, has recently been called into question since energy equipartition is not attained in  $N$ -body simulations except perhaps in their inner cores (BM03; Trenti & van der Marel 2013; Sollima et al. 2015; Bianchini et al. 2016; Spera et al. 2016).
- The functional dependence of the stellar escape rate on the energy required for escape.

- The approximation of a cluster potential by a Plummer (1911) model, all the way out to the tidal radius (which does not exist for a Plummer model).
- An assumed relation between half-mass radius and initial cluster mass, specifically  $r_h \propto M^{0.1}$ . Observed protoclusters, however, have a different relation,  $r_h \propto M^{0.4}$  (Fall et al. 2010).
- The assumption that the half-mass radius  $r_h$  of a cluster remains constant throughout its lifetime. Recent  $N$ -body simulations show this to be an oversimplification. For example,  $r_h$  changes by a factor of  $\sim 6$  during the lifetime of the  $N$ -body model for the globular cluster M4 by Heggie (2014).

We refer the reader to the K09 paper for a full description and justification of these and other ingredients of the K09 model.

As an illustration of uncertainties in the K09 model, we compare its predicted  $M/L$  evolution with that of a corresponding BM03 simulation.<sup>10</sup> We choose this particular comparison because the K09 model predictions were normalized against the BM03 simulations. As shown in Fig. 9, the K09 model predictions follow the BM03 simulation quite well until an age of a few Gyr, after which the  $M/L_V$  decreases significantly in the K09 model whereas it continues to *increase* in the BM03 simulation, especially during the last few Gyr of its lifetime of  $\approx 14$  Gyr. The latter increase, which implies an *increasing*  $M/L$  with *decreasing* luminosity at ages  $\gtrsim 10$  Gyr, is thought to be due to the accumulation of massive white dwarfs in the cluster (see BM03).

The K09 model predictions were normalized against the BM03 simulations by using the same initial conditions (see Sect. 4 in K09). However, the initial conditions in the BM03 simulations differ from those in the published K09 models in one important aspect, namely the upper mass limit of the stellar IMF: BM03 used  $15 M_\odot$  (thus excluding progenitors of stellar-mass black holes), whereas the K09 model uses 100

<sup>10</sup> The properties of this BM03 simulation, shown in their Fig. 18, are:  $W_0 = 5$  and dissolution timescale  $t_0 = 10.7$  Myr (see equation 7 in Kruijssen & Mieske 2009). The properties of the corresponding K09 model are:  $W_0 = 5$  and  $t_0 = 10$  Myr.

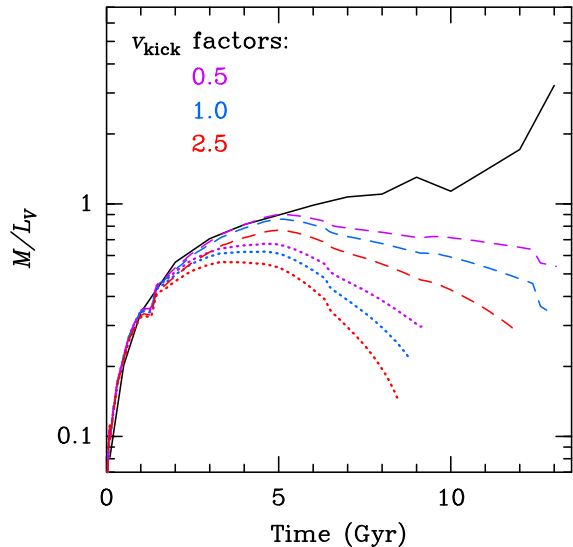


**Figure 9.** *Black line:* evolution of  $M/L_V$  in the  $N$ -body simulation of BM03 for a  $W_0 = 5$  cluster with initial mass  $M_0 = 7 \times 10^4 M_\odot$  and  $t_0 = 10.7$  Myr discussed in Section 5.2. *Dashed lines:* K09 model for a  $W_0 = 5$  cluster with  $M_0 = 10^5 M_\odot$ ,  $t_0 = 10$  Myr, and three factors by which the “standard” kick velocities of dark remnants can be multiplied (0.5, 1.0, and 2.5 in purple, blue, and red, respectively). *Dotted lines:* same as dashed lines, but now for a cluster with  $M_0 = 6 \times 10^4 M_\odot$ .

$M_\odot$ , and includes prescriptions for retention fractions of, and kick velocities applied by, neutron stars and stellar-mass black holes. Fig. 9 illustrates the significant effect of those kick velocities to  $M/L_V$  in the K09 model.

Note that the significant disagreement between  $M/L_V$  in the BM03 simulation and that in the K09 model predictions at ages  $\gtrsim 6$  Gyr exists for all choices of kick velocities. While the analytical implementation of kicks by dark remnants in the K09 model seems plausible at some level, there is significant uncertainty in the retention fractions and kick velocities exerted by white dwarfs, neutron stars, and black holes. Another related simplification in the K09 model is that it applies a given retention fraction of dark remnants throughout the lifetime of a cluster, while  $N$ -body simulations have shown that the retention fraction of stellar-mass black holes can decrease significantly during the lifetime of the cluster due to multiple encounters (Kulkarni et al. 1993; Sigurdsson & Hernquist 1993; Portegies Zwart & McMillan 2000; Merritt et al. 2004; Trenti et al. 2010). Furthermore, the evolution of the retention fraction of black holes varies widely among repeated simulations with the same initial conditions (Merritt et al. 2004). It thus seems fair to conclude that the  $M/L_V$  decrease during the second half of the lifetime of a cluster in the K09 models is not well constrained by observations or simulations.

We emphasize that this comparison between the K09 models and the BM03 simulation tests only a few of the many assumptions listed above. Most of the others remain untested; however, it seems likely that they would also have some impact on the resulting  $M/L$  vs. time and  $M/L$  vs.  $M$  and  $L$  relations.

### 5.3. Ambiguous Evidence from Stellar Mass Functions

One argument in favor of variations in cluster  $M/L$  ratios is that observed stellar MF slopes  $\alpha$  tend to be relatively flat for low-luminosity GCs when compared with those for high-luminosity GCs (Kruijssen & Mieske 2009; KPZ09). We re-examine this argument in this Section by comparing available high-quality data on  $\alpha$  in Galactic GCs with the K09 model

predictions.

Fig. 10 shows  $\alpha$  for a mass function  $dn/dm \propto m^\alpha$  versus  $\log L_V$  from de Marchi et al. (2007), who compiled global MF slopes of 20 GCs in the stellar mass range of  $0.3\text{--}0.8 M_\odot$  derived from *Hubble Space Telescope* (*HST*) data. We assume measurement uncertainties of 0.3 dex for  $\alpha$  (G. de Marchi, private communication). The observed values of  $\alpha$  are compared with predictions of the reference K09 model in Fig. 10.

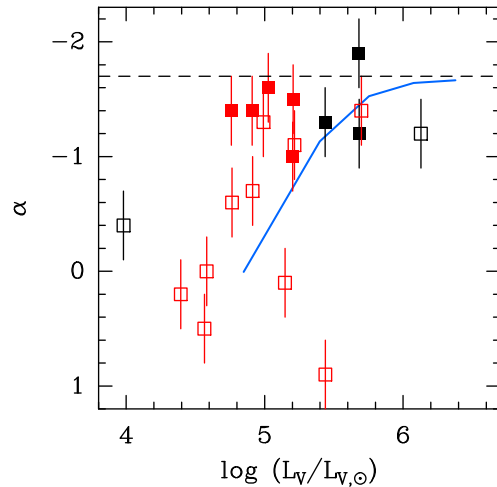


**Figure 10.** Stellar mass function slope  $\alpha$  versus  $\log L_V$  for GCs in the sample of de Marchi et al. (2007). Filled squares and open squares represent GCs with King concentration indices  $c > 1.4$  and  $c < 1.4$  (corresponding to  $W_0 > 6$  and  $W_0 < 6$ ), respectively. GCs with current half-mass relaxation times  $< 1$  Gyr are shown in red while the others are shown in black. The solid blue curve represents the predictions of the reference K09 model. The dashed line indicates  $\alpha = -1.7$ , the mean slope of the Kroupa IMF in the stellar mass range  $0.3\text{--}0.8 M_\odot$ . See the discussion in Sect. 5.3.

As mentioned by KPZ09, GCs in the fainter half of the sample studied by de Marchi et al. (2007) are on average more depleted in low-mass stars than those in the brighter half (see Fig. 10). This trend is, in principle, roughly consistent with the predictions of the reference K09 model. However, it should also be noted that *all* GCs that are significantly depleted in low-mass stars relative to the most luminous GCs feature relatively low King concentration parameters ( $c \equiv \log(r_t/r_c) \lesssim 1.4$ , corresponding to  $W_0 \lesssim 6$ ).<sup>11</sup> Conversely, all GCs with  $W_0 \gtrsim 6$  show  $\alpha$  values consistent with a Kroupa (2001) IMF, and thus do not show any significant trend of  $M/L_V$  with  $L_V$ . The latter does not seem consistent with the predictions of the reference K09 model for the Galactic GC system as a whole, which adopted  $W_0 = 7$ .

However, the strong depletions of low-mass stars seen in GCs with low concentration indices can also be explained in a different way: Baumgardt et al. (2008) argued that this observation may be caused by low-concentration GCs having started out as tidally limited clusters with relatively high levels of primordial mass segregation. The low-mass stars in such clusters would initially be located relatively close to the tidal radius, allowing their evaporation from the cluster to start well before the cluster experiences core collapse, thus leading to present-day mass functions that are relatively strongly depleted in low-mass stars. In this context, we also note that the  $N$ -body simulations by Trenti et al. (2010) showed that GCs

<sup>11</sup> This tendency was already noted by de Marchi et al. (2007) in a diagram of  $\alpha$  versus  $c$  (their Fig. 1). Our Fig. 10 illustrates the luminosity dependence of the difference in  $\alpha$  between GCs with high and low values of  $c$ .

with low initial concentration index ( $W_0 = 5$  or 3) gradually evolve to higher concentration indices ( $W_0 \sim 7$ ) within 40–70% of their dissolution time. As such, low-luminosity GCs with *current* low concentration indices likely had even lower concentration indices initially, which might have caused the strong depletion of low-mass stars in such GCs to start even earlier than predicted by the Baumgardt et al. (2008) study. This effect is not incorporated in the K09 models, rendering it hard to determine the reason for the significant difference in  $\alpha$  between GCs with low and high concentration indices without additional information.

In conclusion, the observed depletion of low-mass stars in low-luminosity GCs can be explained in more than one way and therefore is a weak or inconclusive test of the stellar mass dependence of the escape rate in the K09 models. Hence our conclusions from the previous sections remain valid.

## 6. SUMMARY AND CONCLUSIONS

The most promising explanation for the peaked shape of the observed luminosity function (LF) of old GCs is that it is a relic of dynamical processes—primarily stellar escape driven by internal two-body relaxation—operating on an initial power-law or Schechter MF of young clusters over a Hubble time. The semi-analytical models of FZ01 showed quantitative agreement with the present-day observed GCLF for a wide range of initial MF shapes. For the sake of simplicity, and based on theoretical and observational standard practice at the time, FZ01 adopted an evaporation rate independent of cluster mass and a mass-to-light ratio independent of cluster mass. KPZ09 challenged both of these assumptions. They claimed that the predicted GCLF was only consistent with the observed GCLF if the stellar evaporation rate depends significantly on cluster mass:  $dM/dt \propto M^{1-\gamma}$  with  $\gamma = 0.7$  rather than  $\gamma = 1$  for the FZ01 model. To calculate the escape rates of stars of different masses and hence the variation of  $M/L$  among clusters with different masses, they employed the semi-analytical model of K09, which involves a significant number of plausible, but largely untested, assumptions and approximations.

In this paper, we performed a quantitative evaluation of the KPZ09 claim that their model could fit the observed GCLF while the FZ01 model could not. We conclude that this claim is not valid, based on the following analysis and results.

1. The FZ01 and KPZ09 models provide equally good fits to the observed GCLF in the Milky Way. Furthermore, both models yield a significantly better fit to the observed GCLF at low luminosities than the traditional Gaussian model, highlighting the importance of mass loss driven by two-body relaxation in shaping the GCLF.
2. The measured  $M/L_V$  values of GCs in the Milky Way and the Andromeda galaxy show no dependence on cluster luminosity. At low GC luminosities ( $\log(L_V/L_{V,\odot}) \lesssim 5$ ), where the impact of a stellar mass-dependent escape rate is expected to be strongest, the observations are fitted better by a mass-independent  $M/L_V$  than by the KPZ09 model. This result holds for all six independent studies of GCs with dynamical  $M/L_V$  data analyzed here.
3. We find that the discrepancy between the observed  $M/L_V$  data at low GC luminosities and the KPZ09 predictions cannot be resolved by increasing the character-

istic dissolution timescale  $t_0$  of the K09 model, since such an increase would yield an unacceptable fit to the GCLF. In other words, there is no value of  $t_0$  that allows the K09 model to fit simultaneously the GCLF and the observed  $M/L_V$  data at  $\log(L_V/L_{V,\odot}) \lesssim 5$ .

4. The parameter  $\gamma = 0.7$  adopted by KPZ09 is based on results of  $N$ -body simulations of GCs with initial masses  $M_0 \lesssim 7 \times 10^4 M_\odot$ , whereas the initial masses of GCs that survive 12 Gyr of dynamical evolution are at least one order of magnitude higher than that. Theory indicates that the value of  $\gamma$  will increase toward unity at higher masses. Thus, the appropriate value of  $\gamma$  for models of the GCMF and GCLF evolution may be closer to 1.0 than to 0.7.

We emphasize again that we do not dispute the physical principles of retarded evaporation and  $M/L$  variations. Rather, we claim that these effects add substantially to the complexity of dynamical GCMF and GCLF models and are not needed in practice to match observed GCLFs.

We thank Laura Watkins and the anonymous referee for helpful comments. This project was partially supported by *HST* Program GO-11691 which was provided by NASA through a grant from the Space Telescope Science Institute, which is operated by the Association of Universities for Research in Astronomy, Inc., under NASA contract NAS5–26555. We acknowledge the use of the *R* Language for Statistical Computing, see <http://www.R-project.org>.

## REFERENCES

- Baumgardt, H. 1998, *A&A*, 330, 480  
 Baumgardt, H. 2001, *MNRAS*, 325, 1323  
 Baumgardt, H., de Marchi, G., & Kroupa, P. 2008, *ApJ*, 685, 247  
 Baumgardt, H., & Makino, J. 2003, *MNRAS*, 340, 227 (BM03)  
 Bianchini, P., van de Ven, G., Norris, M. A., Schinnerer, E., & Varri, A. L. 2016, *MNRAS*, 458, 3644.  
 Binney, J., & Merrifield, M. 1998, *Galactic Astronomy* (Princeton, NJ: Princeton University Press)  
 Bruzual, G. A. & Charlot, S. 2003, *MNRAS*, 344, 1000  
 Chabrier, G. 2003, *PASP*, 115, 763  
 Chandar, R., Fall, S. M., & McLaughlin, D. E. 2007, *ApJ*, 668, L119  
 Chandar, R., Whitmore, B. C., & Fall, S. M. 2010, *ApJ*, 713, 1343  
 Christian, C. A., & Schommer, R. A. 1988, *AJ*, 95, 704  
 de Marchi, G., Paresce, F., & Pulone, L. 2007, *ApJL*, 656, L65  
 Dinescu, D. I., Girard, T. M., & van Altena, W. F. 1999, *AJ*, 117, 1792  
 Elson, R. A. W., & Fall, S. M. 1985, *ApJ*, 299, 211  
 Fall, S. M. 2006, *ApJ*, 652, 1129  
 Fall, S. M., & Chandar, R. 2012, *ApJ*, 752, 96  
 Fall, S. M., Krumholz, M. R., & Matzner, C. D. 2010, *ApJL*, 710, L142  
 Fall, S. M., & Rees, M. J. 1977, *MNRAS*, 181, 37P  
 Fall, S. M., & Zhang, Q. 2001, *ApJ*, 561, 751 (FZ01)  
 Fukushige, T., & Heggie, D. C. 2000, *MNRAS*, 318, 753  
 Gnedin, O. Y., & Ostriker, J. P. 1997, *ApJ*, 474, 223  
 Goudfrooij, P. 2012, *ApJ*, 750, 140  
 Goudfrooij, P., Gilmore, D., Whitmore, B. C., & Schweizer, F. 2004, *ApJL*, 613, L121  
 Goudfrooij, P., Schweizer, F., Gilmore, D., & Whitmore, B. C. 2007, *AJ*, 133, 2737  
 Harris, W. E. 1991, *ARA&A*, 29, 543  
 Harris, W. E. 1996, *AJ*, 112, 1487  
 Heggie, D. C. 2014, *MNRAS*, 445, 3435  
 Hénon, M. 1969, *A&A*, 2, 151  
 Innanen, K. A., Harris, W. E., & Webbink, R. F. 1983, *AJ*, 88, 338  
 Kimmig, B., Seth, A., Ivans, I. I., Strader, J., Caldwell, N., Anderson, T., & Gergersen, D. 2015, *AJ*, 149, 53  
 King, I. R. 1962, *AJ*, 67, 471  
 King, I. R. 1966, *AJ*, 71, 64

- Kroupa, P. 2001, *MNRAS*, 322, 231
- Kruijssen, J. M. D. 2009, *A&A*, 507, 1409 (K09)
- Kruijssen, J. M. D., & Mieske, S. 2009, *A&A*, 500, 785
- Kruijssen, J. M. D., & Portegies Zwart, S. F. 2009, *ApJ*, 698, L158 (KPZ09)
- Kruijssen, J. M. D., & Portegies Zwart, S. F. 2010, in *ASP Conf. Ser.* 423, *Galaxy Wars: Stellar Populations and Star Formation in Interacting Galaxies*, ed. B. J. Smith et al. (San Francisco: Astronomical Society of the Pacific), 151
- Kulkarni, S. R., Hut, P., & McMillan, S. L. W. 1993, *Nature*, 364, 421
- Lamers, H. J. G. L. M., Baumgardt, H., & Gieles, M. 2010, *MNRAS*, 409, 305
- Lee, H. M., & Goodman, J. 1995, *ApJ*, 443, 109
- Levenberg, K. 1944, *Quarterly of Applied Mathematics*, 2, 164
- Lützgendorf, N., Kissler-Patig, M., Neumayer, N., et al. 2013, *A&A*, 555, A26
- Mandushev, G., Spassova, N., & Staneva, A. 1991, *A&A*, 252, 94
- Marquardt, M. 1963, *SIAM J. Appl. Math.*, 11, 431
- McLaughlin, D. E. 2000, *ApJ*, 539, 618
- McLaughlin, D. E., & Fall, S. M. 2008, *ApJ*, 679, 1272
- McLaughlin, D. E., & van der Marel, R. P. 2005, *ApJS*, 161, 304
- Merritt, D., Piatek, S., Portegies Zwart, S., & Hemsendorf, M. 2004, *ApJ*, 608, 25
- Meylan, G., & Heggie, D. C. 1997, *A&A Rev.*, 8, 1
- Plummer, H. C. 1911, *MNRAS*, 71, 460
- Portegies Zwart, S. F., & McMillan, S. L. W. 2000, *ApJ*, 528, L17
- Prieto, J. L., & Gnedin, O. Y. 2008, *ApJ*, 689, 919
- Pryor, C., & Meylan, G. 1993, in *ASP Conf. Ser.* 50, *Structure and Dynamics of Globular Clusters*, ed. S. G. Djorgovski & G. Meylan (San Francisco: Astronomical Society of the Pacific), 357
- Schechter, P. 1976, *ApJ*, 203, 297
- Shanahan, R. L., & Gieles, M. 2015, *MNRAS*, 448, L94
- Sigurdsson, S., & Hernquist, L. 1993, *Nature*, 364, 423
- Silverman, B. W. 1986, in *Density Estimation for Statistics and Data Analysis*, Chap and Hall/CRC Press, Inc.
- Sollima, A., Baumgardt, H., Zocchi, A., Balbinot, E., Gieles, M., Hénault-Brunet, V., & Varri, A. L. 2015, *MNRAS*, 451, 2185
- Spera, M., Mapelli, M., & Jeffries, R. D. 2016, *MNRAS*, 460, 317
- Spitzer, L. Jr. 1987, *Dynamical Evolution of Globular Clusters* (Princeton: Princeton University Press)
- Strader, J., Caldwell, N., & Seth, A. C. 2011, *AJ*, 142, 8 (SCS11)
- Trenti, M., & van der Marel, R. 2013, *MNRAS*, 435, 3272
- Trenti, M., Vesperini, E., & Pasquato, M. 2010, *ApJ*, 708, 1598
- van den Bergh, S., & Lafontaine, A. 1984, *AJ*, 89, 1822
- Vesperini, E. 1998, *MNRAS*, 299, 1019
- Vesperini, E., & Heggie, D. C. 1997, *MNRAS*, 289, 898
- Watkins, L. L., van der Marel, R. P., Bellini, A., & Anderson, J. 2015, *ApJ*, 812, 149
- Whitmore, B. C., Chandar, R., Bowers, A. S., Larsen, S., Lindsay, K., Ansari, A., & Evans, J. 2014, *AJ*, 147, 78
- Zaritsky, D., Zabludoff, A. I., & Gonzalez, A. H. 2011, *ApJ*, 727, 116
- Zaritsky, D., Colucci, J. E., Pessev, P. M., Bernstein, R. A., & Chandar, R. 2012, *ApJ*, 761, 93
- Zaritsky, D., Colucci, J. E., Pessev, P. M., Bernstein, R. A., & Chandar, R. 2013, *ApJ*, 770, 121
- Zaritsky, D., Colucci, J. E., Pessev, P. M., Bernstein, R. A., & Chandar, R. 2014, *ApJ*, 796, 71
- Zhang, Q., & Fall, S. M. 1999, *ApJ*, 527, L81

## APPENDIX

SYSTEMATIC DIFFERENCES BETWEEN DYNAMICAL  $M/L$  STUDIES

In this Appendix, we analyze and quantify systematic differences between the five sources of dynamical  $M/L_V$  measurements used in Section 3.1 so that they can be combined in a useful way. The  $M/L_V$  values from McLaughlin & van der Marel (2005) were derived from central velocity dispersions from Pryor & Meylan (1993) which were then extrapolated to “global” values (for the cluster as a whole) using surface brightness profiles. McLaughlin & van der Marel (2005) used single-mass King models in this extrapolation, so that any radial gradients of  $M/L_V$  are neglected. Since ancient GCs commonly display radial mass segregation (e.g., Meylan & Heggie 1997), which causes the more massive stars to be more centrally concentrated than the less massive stars (which have higher  $M/L$ ), we treat  $M/L_V$  values from McLaughlin & van der Marel (2005) as lower limits.

Zaritsky et al. (2012, 2013, 2014) measured velocity dispersions using a drift-scan technique that moved the spectrograph slit across the target cluster during the exposures, covering roughly the region within the half-light radius. The  $M/L_V$  ratios of Zaritsky et al. were determined using an empirical relation between the half-light radius, the average surface brightness within that radius, and the mass-to-light ratio within that radius. This scaling relation was found to apply to all stellar systems from star clusters to massive elliptical galaxies. However, as discussed in Zaritsky et al. (2012), their method produces  $M/L_V$  values that are on average  $\sim 40\text{--}50\%$  lower than those of McLaughlin & van der Marel (2005). This is consistent with the observation that ancient star clusters lie systematically somewhat above the empirical relation used by Zaritsky et al. (see Fig. 2 in Zaritsky et al. 2011).

The kinematic data analyzed by Kimmig et al. (2015) consisted of radial velocities of individual cluster stars, both from new observations and from the literature. GC masses were determined by fitting single-mass King models to the observed radial velocity dispersion profiles. Similar to the case of McLaughlin & van der Marel (2005), we thus treat the  $M/L_V$  values from Kimmig et al. (2015) as lower limits.

Watkins et al. (2015) derived  $M/L_V$  ratios by fitting dynamical models to a combination of proper-motion velocity dispersions (from multi-epoch *HST* imaging data) and spectroscopic line-of-sight velocity dispersions. Their fitting involved Jeans models that assume a constant  $M/L$  ratio, which we therefore formally treat as lower limits. However, the dispersion data used by Watkins et al. (2015) covered a large range of radii, and no assumptions were made regarding the radial luminosity density profile, since they used a Multi-Gaussian Expansion fit to the latter. Hence, their resulting  $M/L$  values can be expected to represent the cluster as a whole relatively well.

Finally, the integrated-light kinematics in Lützgendorf et al. (2013) were derived from integral-field spectroscopy with spatial coverage typically out to the half-light radii of the clusters. Along with surface brightness profiles derived from *HST* data, the  $M/L_V$  values in Lützgendorf et al. (2013) were determined using Jeans modeling. Their method incorporates a correction for radially varying  $M/L_V$  and as such seems likely to produce results that are more robust relative to mass segregation than the other studies mentioned above. From the 11 GCs in common between the studies of Lützgendorf et al. (2013) and McLaughlin & van der Marel (2005), the ratio of the  $M/L_V$  values is  $1.20 \pm 0.10$  where the quoted uncertainty is the standard error of the mean. Similarly, the mean ratio of the  $M/L_V$  values of Lützgendorf et al. (2013) and those of Kimmig et al. (2015) is  $1.26 \pm 0.25$  for the 4 GCs in common between the two studies, whereas that ratio is  $1.07 \pm 0.10$  for the 7 GCs in common between Lützgendorf et al. (2013) and Watkins et al. (2015). For the purposes of this paper, we suggest that these ratios are useful

estimates of the factor by which  $M/L_V$  values may be systematically underestimated in the studies that assumed a constant  $M/L$  throughout the cluster.<sup>12</sup>

Panel (f) of Fig. 2 depicts our corrections for the systematic differences between the  $M/L_V$  estimates of the five studies described above. We adopt the normalization of Lützgendorf et al. (2013). For consistency with this normalization, we multiplied the  $M/L_V$  values of McLaughlin & van der Marel (2005), Zaritsky et al. (2012, 2013, 2014), Kimmig et al. (2015), and Watkins et al. (2015) by factors of 1.20, 1.75, 1.26, and 1.07, respectively.

<sup>12</sup> As mentioned in Sect. 3.1, the level of mass segregation is expected to depend on cluster mass to some extent. We neglect this effect, which is

likely most significant for studies that use central velocity dispersions (e.g., McLaughlin & van der Marel 2005).